European Journal of Molecular & Clinical Medicine

ISSN 2515-8260 Volume 08, Issue 03, 2021

SARS-CoV2 multiple target inhibitors from *Andrographis Paniculata*: An *in-silico* report

Short title: SARS-CoV2 inhibitors from *A.Paniculata*

Karthikeyan Swaminathan[1], Kavinkumar Nirmala Karunakaran[1], Jeevitha priya Manoharan[1], Subramanian Vidyalakshmi [1*]

[1] Department of Biotechnology, PSG College of Technology, Coimbatore - 641 004, Tamilnadu, India

Corresponding author:
Dr. Subramanian Vidyalakshmi *
Mailing address: Department of Biotechnology, PSG College of Technology, Coimbatore-641 004, Tamil Nadu, India
Tel.: 0422-2572177
Mobile phone: +91 9894593378
E-mail: svd.bio@psgtech.ac.in , vids21@gmail.com

Abstract:
Coronavirus Disease – 2019 (COVID–19) caused by the novel coronavirus, SARS-CoV2 has plagued the world in pandemic for the past few months. Currently, many groups are investigating on a potent candidate for treating this highly infectious disease. Phytocompounds from many medicinal plants are reported to possess anti-viral and anti-inflammatory properties. The current study emphasizes on evaluating the inhibition efficacy of the phytocompounds from Andrographis paniculata against 10 structural and non-structural SARS-CoV2 proteins by virtual screening. Molecular docking, binding interactions, ADME and toxicity profiling of the selected fifty one phytocompounds were analysed and compared against 10 well studied repurposed drugs. The best docked complexes were subjected to MD simulation for 50 nanoseconds and the compound stigmasterol was observed to be outperforming in the simulation studies. We report that A.paniculata constitutes 65.78% druggable phytocompounds against SARS-CoV2. We found that the two phytosterols, stigmasterol and stigmasta-5,22-dien-3-ol act as potential lead molecules against multiple target proteins of SARS–CoV2. Based on the literature evidence on Andrographis paniculata and our detailed analysis, this plant and its phytocompounds could be repurposed as a potential anti-COVID agent.

Keywords: SARS-CoV2, Andrographis paniculata, ADME, Molecular Docking, Molecular dynamic simulation.

ISSN 2515-8260 Volume 08, Issue 03, 2021

Introduction:

The novel Coronavirus which causes COVID-19 had dramatically changed the public health wellbeing currently. The virus is the seventh known coronavirus to infect humans and it is officially named as SARS-CoV2 by the Coronavirus Study Group (CSG) of the International Committee on Taxonomy of Viruses [1]. It was first identified in Wuhan in the Hubei province of China [2]. COVID-19 was declared as a pandemic threat by the World Health Organization (WHO) in March 2020 as the number of cases in many countries had increased exponentially. SARS-COV2 has a higher human to human infection rate compared to its predecessor SARS-CoV which caused an epidemic in 2003. Moreover, there is no treatment or cure to curb this virus and this poses tremendous stress in many hospital settings with limited treatment or care.

SARS-CoV2 targets the respiratory system predominantly. The spike protein of the virus gains entry to the human cell via a receptor on the alveolar pneumocytes called Angiotensin Converting Enzyme-2 (ACE-2) [3]. Its single-stranded RNA undergoes replication and transcription with the help of the ribosome and RNA-dependent RNA polymerase enzyme (RdRp) upon attachment. Thus, the viral proteins and its RNA genome are synthesized and assembled in the cell, resulting in the replication of the virus. In this way, the virus affects millions of pneumocytes in the lungs. The damaged cell triggers a cascade of inflammatory mediators causing vasodilation and increased capillary permeability of affected cells. The immune reaction wards off the virus but also damages the healthy cells in the vicinity. In few patients, the inflammation gets uncontrollable, leading to excess healthy tissues damage and organ failure which in turn drives the patient to death [4], [5]. This is evident in critical patients who die due to Acute Respiratory Distress Syndrome (ARDS) because of cytokine storm. Researchers have also shown that ageing people with COVID-19 and people suffering from COVID-19 along with other co-morbidities have increased chances of being critically affected.

The WHO had started the "Solidarity" clinical trials for drugs against SARS-COV2 under which three treatment options are being studied: Remdesivir, Lopinavir/Ritonavir with and without interferon beta 1a. These anti-viral drugs were used to treat Ebolavirus and Human Immunodeficiency Virus and these may have some effects on the new coronavirus. Treatment using Chloroquine and Hydroxychloroquine was halted in May and June 2020 respectively as they showed no improvements in treating the patients [6]. Clinical trials in the United Kingdom showed that Dexamethasone, a promising corticosteroid, reduced the mortality by a third in patients requiring ventilators and by a fifth for patients requiring only oxygen [7].

Traditionally, plants are used as medicines for a wide variety of chronic diseases and found to possess diverse anti-viral properties. They have been used since the dawn of human civilization because of their non-toxicity, lesser side effects, cost effectiveness and the ease of availability as compared with the synthetic drugs [8]. One such herbal plant is the *Andrographis paniculata* (English:Green Chirayta, Tamil: Nilavembu) which is well known for its pharmacological attributes. The extract of this herb constitutes a major part in Kabasura kudineer which is suggested by the traditional medicine practitioners in India for aiding our immune system to fight against SARS-COV2. Numerous phytocompounds of *A.paniculata* were reported to be highly active against viral infections. It is also known for

its anti-inflammatory, anti-diarrheal, thrombolytic, hepatoprotective and anti-pyretic properties [9], [10], [11]. Hence, we focused on exploring the antiviral property of the phytocompounds of *A. Paniculata* against SARS-COV2.

As of 16th Jan 2020, a total of 1413 SARS–CoV2 protein structures have been deposited at RCSB Protein Data Bank [12]. The proteins namely Non-Structural Proteins (NSP) 3, NSP 5 (main protease), NSP 9 and NSP15, Spike protein, Envelope protein, Membrane protein, Receptor Binding protein, ORF3a Accessory protein and ORF1a polyprotein were identified to be potential drug targets since the emergence of SARS-CoV2. These protein targets were reported to be involved in various key mechanisms such as viral attachment, transcription, replication and viral synthesis, ion channel formation for the release of viral particles, RNA binding proteins, host's RNA translation blockers, cytokine expression promoters and as dominant immunogens [13-18]. Our study includes these critical proteins as targets for identifying therapeutic candidates against SARS-CoV2.

Virtual docking was performed for analyzing the interaction of these phytocompounds with the structural and non-structural proteins of the virus. Current FDA approved repurposed drugs are also included in this study. We highly consider that the outputs of this study could throw some light in the drug development strategies for SARS-CoV2.

Materials and methods Ligand selection

A total of fifty-one phytocompounds present in *A.paniculata* were selected through an extensive literature analysis and phytocompound databases analysis [19]. The list of phytocompounds from *A.paniculata* and the repurposed drugs are listed in Table 1. The 3D structures of the phytocompounds and the drugs were retrieved from PubChem (https://pubchem.ncbi.nlm.nih.gov/), ChemSpider (www.chemspider.com) and Drug Bank (www.drugbank.com). The structures of these ligands were downloaded in the SDF format. The compounds lacking the structures in the above-mentioned databases were excluded from the study. The chemical structures of the ligands are given in supplementary table S1.

Evaluation of the drug likeliness of ligands

An online tool SWISSADME (http://www.swissadme.ch/) was used to predict the Absorption, Distribution, Metabolism and Excretion (ADME) parameters and drug-like nature of the selected ligands [20]. For the phytocompounds to be eligible for molecular docking analysis, the compounds must satisfy the Lipinski rule of five which generally helps to distinguish compounds possessing drug-like properties with other counterparts possessing no drug-like properties [21]. Lipinski rule of five includes the following criteria for drug likeness: 1) molecular mass should be less than 500 Dalton, 2) possess high lipophilicity (expressed as Log P less than 5), 3) should have less than 5 hydrogen bond donors, 4) should have less than 10 hydrogen bond acceptors and 5) have a molar refractivity in the range of 40-130. The phytocompounds which passed the rule of five were taken for docking analysis.

Ligand preparation

The ligands are converted from SDF format to PDB format using Open Babel v3.1.1

software [22]. The PDB format of the ligands were uploaded to the Avogadro v1.2.0 and were energy minimized [23]. The ligands were saved again in PDB format and then uploaded to the MGL Tools v1.5.6 software. The number of rotatable bonds was noted. The missing hydrogen atoms were added to the ligands and the bond orders were corrected. Gasteriger charges were automatically added by the MGL Tools to the ligand and the Non-polar hydrogen atoms were merged. The root of the ligand was then detected under the Torsion tree option and the prepared ligand was saved in PDBQT format. The PDBQT file of the ligands was used for the docking studies. The same procedure was followed for the repurposed drugs.

SARS-CoV2 target proteins selection and preparation

Ten high resolution target proteins of SARS-CoV2 (Protein PDB IDs: 6LU7, 6WXD, 5X29, 2G9T, 6M0J, 3I6G, 6VXS, 6XDC, 6VWW and 6CRV) were used for docking studies (Table 2). The three-dimensional structures of the target proteins were sourced from RCSB Protein Data Bank and were downloaded in the PDB format. The active sites of the receptor proteins were predicted using Metapocket 2.0 [24], [25] and Computed Atlas of Surface Topography of proteins (CASTp) [26]. The coordinate data of the first cavity predicted by the Metapocket 2.0 were chosen for grid generation. Similarly, the amino acid residues mentioned in the top hit of CASTp result were considered for setting up the receptor grid box. The protein PDB file was uploaded to the MGL Tools v1.5.6 software for the protein preparation. The water molecules were deleted in the protein, and polar hydrogen and Kollman charges were added. The prepared target proteins were saved as PDBQT file for the grid generation. Grid box parameters of the target proteins are listed in Table 2.

Molecular docking analysis

Phytocompounds which passed the ADME test were included in the molecular docking studies. The active site position and grid parameters were specified in the configuration file for docking. Both the phytocompounds and the positive controls were then docked with the selected 10 proteins using Autodock Vina v1.1.2 [27]. The binding affinities were displayed in the generated log file for 10 different ligand-protein interaction positions. The phytocompounds exerting a docking score lower than -7.0 kcal/mol (threshold) against SARS-CoV2 viral proteins were considered for further studies. 2D interaction profile of the docked complexes was investigated using Ligplot+ v1.4.5 [28].

Prediction of pharmacokinetic properties

The molecules chosen from molecular docking studies were then assessed for their ADME and toxicity profile with the help of pkCSM online tool [29]. Canonical SMILES of the selected compounds were given as input for pharmacokinetic prediction. Few significant pharmaceutical parameters like gastro-intestinal absorption (GI), blood-brain barrier permeation (BBB), CYP3A4 substrate and inhibition, total clearance, AMES toxicity test and hepatotoxicity were evaluated. The molecules tested positive in AMES and hepatotoxicity were excluded and the remaining phytocompounds were considered to be potential anti SARS-CoV2 lead molecules.

Prime MM/GBSA calculations

The relative binding affinity of the best docked ligand (stigmasterol) was calculated using molecular mechanics with generalized born surface area (MM/GB-SA). The MM/GBSA was performed using Prime MMGBSA module of the Schrodinger suite (30). The dG binds of the protein -ligand complexes were estimated according to the following equation:

$$E_{Binding} = E_{Complex} - E_{Protein} - E_{Ligand}$$

The obtained energies were then computed using OPLSAA force field. As receptor binding domain (PDB ID: 6M0J) and main Protease (NSP 5) (PDB ID: 6LU7) are reported as major drug targets of coronavirus, the Molecular dynamic behavior of stigmasterol with these proteins were studied thereafter.

Molecular Dynamic simulation

Molecular Dynamic Simulations were performed for the complexes main protease: Stigmasterol and receptor binding domain: stigmasterol . The conformational changes of the protein-ligand complexes with respect to time were observed using Desmond v3.6 package (31). System builder function was used for adjusting the solvation parameters. OPLS3e force field was chosen to mimic the water molecules. Simple point charge model and orthorhombic periodic boundary conditions (Repeating units at 10Å distances) were defined. Ionic regions were not excluded during the run and the entire system was neutralized by adding 17Cl^- ions. Isothermal-isobaric (NPT) ensemble was fixed to perform the MD simulation. Temperature and pressure were maintained at 300K and 1.01325 bars respectively. Salt was not added during the entire run and the model system was relaxed before simulation. MD simulation was made to run for 50 nano seconds at 4.8ps intervals and the MD trajectories were analyzed.

Results and Discussion

Since ancient times, medicinal plants and their extracts have been used to treat and cure several diseases. Earlier studies revealed that phytocompounds might act as good therapeutic agents to treat many infectious diseases [32]. There are also studies which have shown that phytocompounds are effective against HIV [33], Polio virus [34], Dengue virus [35] and influenza virus [36]. Several phytocompounds exhibit anti-viral activity against these viruses by specifically targeting viral proteins in the host cells. These compounds are found to be clinically safe in humans [37], [38]. With the recent growing possibility of the emergence of new coronavirus strains, there is an immediate requirement for effective drugs against this life-threatening virus. In the current scenario, computational drug discovery methods are preferred over the traditional approaches, due to time constraint. Structure based methods like Protein-ligand docking analysis aids in efficient drug discovery [39], [40]. In our present study, 51 phytocompounds from *A. paniculata* were assessed for their potential to act as anti-COVID-19 lead molecules. These were tested against 10 SARS-CoV2 proteins. The target proteins included the proteins needed for viral entry into the host and proteins essential for replication, assembly and synthesis of viral RNAs. A pie chart representation of the ligand selection and ADME screening is shown in Figure 1. Phytocompounds were screened against the target proteins and checked for their ADME properties. BBB penetration barrier separates the circulating blood from the

cerebrospinal fluid in the central nervous system (CNS) and the drug which does not reach the CNS is considered to be more effective [41]. In that way, the identified lead molecules were found to be negative towards CNS activity and hence suggesting the safe usage of these lead molecules as drugs.

Drug likeliness prediction

Out of the fifty-one phytocompounds, ten phytocompounds were found to have no structures or canonical smiles in any of the small molecule databases and therefore these compounds were excluded from our study. Andrographiside, Andrographidine D and Andrographidine F failed to pass the drug likeliness test and were also excluded from our study. Thirty-eight ligands were further analysed by molecular docking. The Lipinski rule of five parameters of these phytocompounds is listed in table 3.

Molecular Docking:

Protein-ligand docking studies were carried out for the selected ten viral protein targets with the thirty-eight phytocompounds and 10 repurposed drugs. The docking grid was generated based on the active site pocket predicted by Metapocket 2.0 and CASTp. The coordinates predicted at the top hit were noted for each protein. Prepared protein and the ligands were docked using Autodock Vina v1.1.2 docking software. A majority of the phytocompounds possessed good binding affinity towards the target proteins. It was observed that more than thirty ligands had a binding affinity lower than -7.0 kcal/mol. The docking scores of the phytocompounds with the 10 target proteins of SARS- CoV2 ranged from -9.9 to -3.7 kcal/mol (Table 4), whereas for the repurposed drugs the scores ranged between -11.6 and -.7 (Table 5). From our analysis, it was seen that the most potent inhibitor for the main protease are Stigmasta-5,22-dien-3-ol and Stigmasterol (-7.8 kcal/mol), whereas among the repurposed drugs, Ivermectin showed highest inhibitory potential (-9.1 kcal/mol). Stigmasta-5,22-dien-3-ol and Stigmasterol also showed the highest docking scores against the membrane protein (-9.9 kcal/mol), NSP9 (-7.8 kcal/mol) and envelope protein (-9.1 kcal/mol). Among the repurposed drugs, Ivermectin was found to possess the most favorable docking scores against multiple proteins like envelope protein (-11.6 kcal/mol), ORF 1a (-9.1 kcal/mol), membrane protein (-10.7 kcal/mol), NSP 15 (-11.1 kcal/mol) and the spike RBD complex (-11.6 kcal/mol). For the spike protein-RBD complex, the phytocompounds, Neoandrographolids and Stigmasterol showed the top binding score (-8.8 kcal/mol). Among the repurposed drugs, Saquinavir showed highest binding affinity with the Spike protein–RBD complex (-9.9 kcal/mol). It was also observed that a majority of the ligands showed favorable docking interaction with all the target proteins. It is evident from the heat map (Fig. 2) that the proteins which had a higher docking score with multiple drug leads are clustered together [42]. For example, spike protein–RBD complex and Main protease are clustered together. Both these had similar interactions with the lead molecules and also possessed similar docking scores. Similarly, spike protein and the main protease forms the next closely clustered proteins. This indicates that the top performing phytocompounds from *A.paniculata* have a high potential to inhibit crucial molecular targets of SARS-CoV2.

On the other hand, ORF3a and NSP9 which showed very less lead molecule scores were

distantly related as orphans in the dendrogram. Interestingly, the top scoring ligands from *A. paniculata* were closely clustered. As evident from Table 6, Stigmasta-5,22-dien-3-ol and Stigmasterol,possessed similar docking scores with multiple target proteins. The same pattern was observed for the pair: Andrographidine A and Andrographidine C. One of the previous study reported that Andrographolide, a well characterized phytocompound of *A. paniculata* had a binding affinity of -3.3 kJ/mol and it might act as an inhibitor for the main protease of SARS-CoV-2 [43]. Another in-vitro study also reported that Ivermectin inhibited the replication of SARS-CoV-2 in vero-hSLAM cells [44].

Analysis of the binding interactions of the phytocompounds and drugs against target proteins

Hydrogen bonding and hydrophobic interactions of the top scoring phytocompounds and repurposed drugs with the viral protein complexes were analysed. The top scoring phytocompounds showed similar interactions with the target proteins. For example, with the main protease, the ligands Stigmasterol and Stigmasta-5,22-dien-3-ol showed similar interacting residues and hydrogen bond contacts. Several of these interacting residues were also shown by the repurposed drugs and hence, indicates similar mode of action. The drug Ivermectin which showed the best docking score against the spike protein, showed no common residues with the top scoring phytocompounds against this protein. This could indicate a variation in the mechanism of action of the drug molecule and the phytochemical leads.

Toxicity Prediction

pkCSM, an online tool was used for predicting the toxicity profile of the phytocompounds under study. The ligands which passed AMES toxicity and Hepatotoxicity were considered for assessing their ADME properties (Table 7). Phytocompounds such as 14-Deoxy-11-oxoandrograpolide, 3-o-caffeoyl-D-quinic acid, Neoandrographolide, Paniculide-A, Paniculide-B, and Paniculide-C were excluded, as they showed possess unacceptable hepatotoxicity and AMES toxicity. Twenty-five phytocompounds passed the toxicity analysis and they could work as potential lead molecules for targeting the SARS-CoV2 proteins. Important pharmacokinetic properties such as Blood-Brain barrier (BBB), $CaCO_2$-permeability, human Ether-a-go-go-Related Gene (hERG I & II) inhibition, AMES toxicity, number of hydrogen bond donors, number of H-bond acceptors, central nervous system (CNS) permeability, molecular weight, human oral absorption and CYP inhibition were also predicted for the potential lead molecules. These properties of the potential lead molecules are reported. Other relevant pharmacokinetic properties of the potential lead molecules were also analysed and listed in supplementary table S2. Through the toxicity analysis, it can be determined that the phytocompounds of the plant *Andrographis paniculata* may constitute 65.78 % of druggable phytocompounds (Figure 3).

Molecular mechanics-generalized Born and surface area (MMGB-SA)

Stigmasterol was docked with the target proteins of SARS-CoV2 at extra precision mode (XP) using the Glide module of Schrodinger suite (Data not shown). The docked pose of

the ligand 34 (stigmasterol): Target proteins were subjected to MM-GBSA calculation for predicting the binding free energy. MMGBSA-dG bind for the Ligand 34: Target Protein complexes are shown in Table 8.

Molecular simulation

The stability of the protein-ligand complexes was determined by molecular dynamic simulation for 50nanoseconds using the DESMOND package of Schrödinger suite. Stigmasterol, having a good binding affinity towards most of the target proteins were subjected to MD simulation. The dynamic characteristics of stigmasterol with target proteins Main protease and Receptor binding domain were studied. Few significant parameters such as root mean square deviation (RMSD), root mean square fluctuations (RMSF), Protein-Ligand contacts and Ligand torsion profile were analyzed.

The conformational and the structural changes of the backbone atoms of the target proteins main protease and receptor binding domain (PDB ID :6LU7 and PDB ID :6M0J) and the Protein: ligand complexes (Main protease: Stigmasterol and Receptor binding domain: Stigmasterol) were monitored by RMSD analysis. The RMSD plot of the native protein and protein: ligand complexes are shown in Figure 4. Main protease: Stigmasterol complex. The RMSD of the free protein was maintained around 2.4 Å. The RMSD of the protein fit ligand was observed to be stable till 30 nanoseconds, however fluctuated towards the end of the simulation (>35 nanoseconds). over all ,analysis of the RMSD profile of the protein and ligand complex indicated the unstable nature of the complex. Receptor binding domain: Stigmasterol complex -The RMSD of the free protein was maintained around 2.4 Å. Though, the RMSD of the protein bound ligand was found to be unstable during the first 9 nanoseconds, later (>10 nanoseconds) maintained a stable conformation till the end of the simulation. Therefore, the observations on the RMSD profile of the protein ligand complex shows that the conformational stability of the complex was maintained throughout the entire simulation.

The Root Mean Square Fluctuation (RMSF) of main protease and receptor binding domain (PDB ID :6LU7 and PDB ID :6M0J) characterizes the local changes of amino acids of protein that occur upon ligand (Stigmasterol) binding. The peaks in the plot indicates the areas that fluctuate the most during the simulation (Supplementary figure 1). The total secondary structure elements (SSE) such as alpha-helices and beta-strands present in the main protease and receptor binding domain (PDB ID :6LU7 and PDB ID :6M0J) were monitored throughout the simulation trajectory. The plot (supplementary figure 2) summarizes the SSE composition for each frame over the entire simulation time. The ligand RMSF showed the fluctuations of internal atoms upon protein binding (Supplementary figure 3). The C_{30} atom of Stigmasterol showed a greater fluctuation upon binding of main protease and receptor binding domain (PDB ID : 6LU7 and PDB ID :6M0J). The solvent exposure is one of the reasons behind the fluctuations of the internal atoms of the ligand. Whereas other atoms of the Stigmasterol are localized firmly at the binding pocket of the target proteins and hence showed no fluctuations.

The ligand Stigmasterol forms hydrogen bond with the residues LEU287, ALA285, MET276, ASN277 and TYR239 of main protease (PDB ID: 6LU7) and LYS 74, ASN 103 of receptor binding domain (PDB ID :6M0J). The residues that were involved in water

bridge formation and ionic interactions are shown in figure 5. Strong hydrophobic interactions were observed with residues TYR237, LEU272, LEU287, LEU286 and TYR239 of main protease (PDB ID: 6LU7) protein.

On the other hand, stigmasterol forms hydrophobic interactions with residues LEU391, PHE40, LEU73, TRP69, LEU100, ALA99 and PHE32 of receptor binding domain (PDB ID: 6M0J). A timeline representation of the protein and ligand contact is represented in figure 6. Moreover, residues ASN 274 of main protease and GLN 102 of receptor binding domain observed to have a negligible interaction with Stigmasterol.

Seven rotatable bonds were present in the ligand Stigmasterol. The conformational changes of each rotatable bond of the ligand during the entire simulation of 50 nanoseconds is summarized in the ligand torsion plot (supplementary figure 4). The dial plot and a bar plot in the figure gives the torsion potential information. This plot also depicts the various conformational strains that a ligand undergoes for maintaining a protein-bound conformation.

On assessing the stability of the protein :ligand complexes. It could be observed that the ligand (Stigmasterol) maintains a stable configuration with receptor binding domain (PDB ID: 6M0J) than main protease (PDB ID:6LU7) throughout the entire simulation period of 50 nanoseconds.

Conclusion

Our analysis involved an exhaustive systematic approach for identifying potential anti-SARS-CoV2 lead phytocompounds from *A.paniculata*. 51 phytocompounds from *A.paniculata* and 10 repurposed drugs were subjected to molecular docking against multiple SARS-CoV2 target proteins. From the analysis, we found that *Andrographis paniculata* had a drugability percentage of 65.78 against the novel coronavirus target proteins. The two-top scoring phytosterols, Stigmasterol and Stigmasta-5,22-dien-3-ol were effective against multiple target proteins. Although the scores were slightly lesser than few of the repurposed drugs, these two phytosterols possess a very high lipophilicity and hence are very good drug candidates. Moreover, the molecular dynamic simulation studies gave insights on the stable nature of the protein and ligand complexes (Main protease: Stigmasterol and receptor binding domain: Stigmasterol) . Several of the ligands were also active against multiple target proteins, which offer a major advantage against escaping drug resistance and molecular mimicry by the virus. To conclude, these phytocompounds could target the virus by multiple mechanisms simultaneously and hence help provide better therapeutic benefits against SARS-CoV2. These phytocompounds could be further explored by in-vitro and in-vivo studies for its inhibitory action against SARS-CoV2.

References

1. Gorbalenya AE, Baker SC, Baric R, de Groot RJ, Drosten C, Gulyaeva AA et al (2020) Severe acute respiratory syndrome-related coronavirus: The species and its viruses – a statement of the Coronavirus Study Group. BioRxiv.
2. Zhou P, Yang XL, Wang XG, Hu B, Zhang L, Zhang W, Si HR, Zhu Y, Li B, Huang CL, Chen HD, Chen J, Luo Y, Guo H, Jiang RD, Liu MQ, Chen Y, Shen XR, Wang X, Zheng XS et al (2020) A pneumonia outbreak associated with a new coronavirus of

probable bat origin. Nature, 579(7798), 270–273. https://doi.org/10.1038/s41586-020-2012-7

3. Du L, He Y, Zhou Y, Liu S, Zheng BJ, & Jiang S (2009) The spike protein of SARS-CoV - A target for vaccine and therapeutic development. Nature Reviews Microbiology, 7(3). https://doi.org/10.1038/nrmicro2090
4. Coperchini F, Chiovato L, Croce L, Magri F & Rotondi M (2020) The cytokine storm in COVID-19: An overview of the involvement of the chemokine/chemokine-receptor system. Cytokine & Growth Factor Reviews, 53, 25-32. https://doi.org/10.1016/j.cytogfr.2020.05.003
5. Yuki K, Fujiogi M & Koutsogiannaki S (2020) COVID-19 pathophysiology: A review. Clinical immunology (Orlando, Fla.), 215, 108427. https://doi.org/10.1016/j.clim.2020.108427
6. "Solidarity clinical trial for COVID-19 treatments - WHO." https://www.who.int/emergencies/diseases/novel-coronavirus-2019/global-research-on-novel-coronavirus-2019- ncov/solidarity-clinical-trial-for-covid-19-treatments (accessed Jul. 05, 2020).
7. RECOVERY Collaborative Group, Horby P, Lim WS, Emberson JR, Mafham M, Bell JL, Linsell L, Staplin N et al (2020) Dexamethasone in Hospitalized Patients with Covid-19 - Preliminary Report. The New England journal of medicine, 10.1056/NEJMoa2021436. Advance online publication. https://doi.org/10.1056/NEJMoa2021436
8. Wachtel-Galor S, Benzie IFF. Herbal Medicine: An Introduction to Its History, Usage, Regulation, Current Trends, and Research Needs. In: Benzie IFF, Wachtel-Galor S, editors. Herbal Medicine: Biomolecular and Clinical Aspects 2nd edition. Boca Raton (FL): CRC Press/Taylor & Francis; 2011. Chapter 1. Available from: https://www.ncbi.nlm.nih.gov/books/NBK92773/
9. Kataky A, Handique PJ (2010) A brief overview on Andrographis paniculata (Burm. f) Nees., a high valued medicinal plant: boon over synthetic drugs. Asian J. Sci. Technol., vol. 6, pp. 113-118.
10. Gupta S, Mishra KP & Ganju L (2017) Broad-spectrum antiviral properties of andrographolide. Arch Virol 162, 611–623. https://doi.org/10.1007/s00705-016-3166-3
11. Subash KR (2020) In silico pharmacokinetic and toxicological properties prediction of bioactive compounds from Andrographis paniculata. doi:10.5455/njppp.2020.10.02040202022042020
12. RCSB PDB: Homepage. https://www.rcsb.org/ (accessed Jul. 15, 2020).
13. Chen Y, Liu Q & Guo D (2020) Emerging coronaviruses: Genome structure, replication, and pathogenesis. Journal of medical virology, 92(4), 418–423. https://doi.org/10.1002/jmv.25681
14. Fehr AR & Perlman S (2015) Coronaviruses: an overview of their replication and pathogenesis. Methods in molecular biology (Clifton, N.J.), 1282, 1–23. https://doi.org/10.1007/978-1-4939-2438-7_1
15. Liu J, Sun Y, Qi J, Chu F, Wu H, Gao F, Li T, Yan J & Gao GF (2010) The membrane protein of severe acute respiratory syndrome coronavirus acts as a dominant immunogen revealed by a clustering region of novel functionally and structurally defined cytotoxic T-lymphocyte epitopes. The Journal of infectious diseases, 202(8),

1171–1180. https://doi.org/10.1086/656315

16. Surya W, Li Y & Torres J (2018) Structural model of the SARS coronavirus E channel in LMPG micelles. Biochimica et biophysica acta.
17. Lan J, Ge J, Yu J, Shan S, Zhou H, Fan S, Zhang Q, Shi X, Wang Q, Zhang L, Wang X (2020) Structure of the SARS-CoV-2 spike receptor-binding domain bound to the ACE2 receptor. Nature. 581. 10.1038/s41586-020-2180-5.
18. Lu W, Zheng BJ, Xu K, Schwarz W, Du L, Wong CK, Chen J, Duan S, Deubel V & Sun B (2006) Severe acute respiratory syndrome-associated coronavirus 3a protein forms an ion channel and modulates virus release. Proceedings of the National Academy of Sciences of the United States of America, 103(33), 12540–12545. https://doi.org/10.1073/pnas.0605402103
19. U.S. Department of Agriculture, Agricultural Research Service. 1992-2016. Dr. Duke's Phytochemical and Ethnobotanical Databases. Home Page, http://phytochem.nal.usda.gov/ http://dx.doi.org/10.15482/USDA.ADC/1239279
20. Daina A, Michielin O & Zoete V (2017) SwissADME: a free web tool to evaluate pharmacokinetics, drug-likeness and medicinal chemistry friendliness of small molecules. Sci Rep 7, 42717. https://doi.org/10.1038/srep42717
21. Lipinski CA, Lombardo F, Dominy BW & Feeney PJ (2001) Experimental and computational approaches to estimate solubility and permeability in drug discovery and development settings. Advanced drug delivery reviews, 46(1-3), 3–26. https://doi.org/10.1016/s0169-409x(00)00129-0
22. O'Boyle NM, Banck M, James CA, Morley C, Vandermeersch T & Hutchison GR (2011) Open Babel: An open chemical toolbox. Journal of cheminformatics, 3, 33. https://doi.org/10.1186/1758-2946-3-33
23. Hanwell MD, Curtis DE, Lonie DC, Vandermeersch T, Zurek E & Hutchison GR (2012) Avogadro: an advanced semantic chemical editor, visualization, and analysis platform. Journal of cheminformatics, 4(1), 17. https://doi.org/10.1186/1758-2946-4-17
24. Huang B (2009). MetaPocket: a meta approach to improve protein ligand binding site prediction. Omics : a journal of integrative biology, 13(4), 325–330. https://doi.org/10.1089/omi.2009.0045
25. Zhang Z, Li Y, Lin B, Schroeder M & Huang B (2011) Identification of cavities on protein surface using multiple computational approaches for drug binding site prediction. Bioinformatics (Oxford, England), 27(15), 2083–2088. https://doi.org/10.1093/bioinformatics/btr331
26. **Tian et al., Nucleic Acids Res. 2018. PMID:** 29860391 **DOI:** 10.1093/nar/gky473**.**
27. Trott O & Olson AJ (2010) AutoDock Vina: improving the speed and accuracy of docking with a new scoring function, efficient optimization, and multithreading. Journal of computational chemistry, 31(2), 455–461. https://doi.org/10.1002/jcc.21334
28. Laskowski RA & Swindells MB (2011) LigPlot+: multiple ligand-protein interaction diagrams for drug discovery. Journal of chemical information and modeling, 51(10), 2778–2786.https://doi.org/10.1021/ci200227u.
29. Pires DE, Blundell TL & Ascher DB (2015) pkCSM: Predicting Small-Molecule

Pharmacokinetic and Toxicity Properties Using Graph-Based Signatures. Journal of medicinal chemistry, 58(9), 4066–4072. https://doi.org/10.1021/acs.jmedchem.5b00104

30. Schrodinger Release 2018-1. (2018f). Prime, Schrodinger, LLC, New York, NY.
31. Schrodinger Release 2018-1. (2018g). Desmond molecular dynamics sys-tem, D. E. Shaw Research, New York, NY, 2018. Maestro-Desmond Interoperability Tools, Schrodinger, New York, NY.
32. Greenwell M & Rahman PK (2015) Medicinal Plants: Their Use in Anticancer Treatment. Internationaljournal of pharmaceutical sciences and research, 6(10), 4103–4112. https://doi.org/10.13040/IJPSR.0975-8232.6(10).4103-12
33. Gyuris A, Szlávik L, Minárovits J, Vasas A, Molnár J & Hohmann J (2009) Antiviral activities of extracts of Euphorbia hirta L. against HIV-1, HIV-2 and SIVmac251. In vivo (Athens, Greece), 23(3), 429–432.
34. Soltan MM & Zaki AK (2009) Antiviral screening of forty-two Egyptian medicinal plants. Journal of ethnopharmacology, 126(1), 102–107. https://doi.org/10.1016/j.jep.2009.08.001
35. Fang CY, Chen SJ, Wu HN, Ping YH, Lin CY, Shiuan D, Chen CL, Lee YR & Huang KJ (2015) Honokiol, a Lignan Biphenol Derived from the Magnolia Tree, Inhibits Dengue Virus Type 2 Infection. Viruses, 7(9), 4894–4910. https://doi.org/10.3390/v7092852
36. Droebner K, Ehrhardt C, Poetter A, Ludwig S & Planz O (2007) CYSTUS052, a polyphenol-rich plant extract, exerts anti-influenza virus activity in
37. Seal A, Aykkal R, Babu RO & Ghosh M (2011) Docking study of HIV-1 reverse transcriptase with phytochemicals. Bioinformation, 5(10), 430–439. https://doi.org/10.6026/97320630005430
38. Senthilvel P, Lavanya P, Kumar KM, Swetha R, Anitha P, Bag S, Sarveswari S, Vijayakumar V, Ramaiah S & Anbarasu A (2013) Flavonoid from Carica papaya inhibits NS2B-NS3 protease and prevents Dengue 2 viral assembly. Bioinformation, 9(18), 889–895. https://doi.org/10.6026/97320630009889
39. Sato H, Shewchuk LM & Tang J (2006) Prediction of multiple binding modes of the CDK2 inhibitors, anilinopyrazoles, using the automated docking programs GOLD, FlexX, and LigandFit: an evaluation of performance. Journalof chemical information and modeling, 46(6),2552–2562. https://doi.org/10.1021/ci600186b
40. Mulukuri NVLS, Dinesh BM, Jha DK, Prabhakar T (2020) Molecular docking and toxicity studies of series of compounds from diaryl urea hits & spiro piperidine indolinyl series as potential p2y1 receptor antagonists. Int J Pharm Sci & Res , 11(4): 1934-40. doi: 10.13040/ IJPSR.0975-8232.11(4).1934-40.
41. Sarah E, Mélina G, Sonia G, Anna G Encyclopedia of Clinical Neuropsychology, Archives of Clinical Neuropsychology, Volume 28, Issue 1, February 2013, Page 92, https://doi.org/10.1093/arclin/acs103
42. Babicki S, Arndt D, Marcu A, Liang Y, Grant JR, Maciejewski A & Wishart DS (2016) Heatmapper: web-enabled heat mapping for all. Nucleic acids research, 44(W1), W147–W153. https://doi.org/10.1093/nar/gkw419

43. Enmozhi SK, Raja K, Sebastine I & Joseph J (2020) Andrographolide as a potential inhibitor of SARS-CoV-2 main protease: an in silico approach. Journal of biomolecular structure & dynamics, 1–7. Advance online publication. https://doi.org/10.1080/07391102.2020.1760136
44. Caly L, Druce JD, Catton MG, Jans DA & Wagstaff KM (2020) The FDA-approved drug ivermectin inhibits the replication of SARS-CoV-2 in vitro. Antiviral research, 178, 104787. https://doi.org/10.1016/j.antiviral.2020.104787

Table 1: List of Phytocompounds from *Andrographis paniculata* and FDA approved drugs (Positive Controls)

S.No	Compounds	Source	CID	Chemical formula
1	14-Deoxy-11,12-didehydroandrographolide	PubChem	5708351	C20H28O4
2	14-Deoxy-11-oxoandrographolide	PubChem	101593061	C20H28O5
3	14-Deoxyandrographolide	PubChem	11624161	C20H30O4
4	14-Deoxyandrographoside	PubChem	44575270	C26H40O9
5	2,4-Dihydroxycinnamic acid	PubChem	446611	C9H8O4
6	3-o-Caffeoyl-d-quinic acid	PubChem	1794426	C16H17O9-
7	5-hydroxy-3,7,8-trimethoxy-2-(2-methoxyphenyl)-4h-chromen-4-one	ChemSpider	24845625	C19H18O7
8	5-Hydroxy-7,8,2',3'-tetramethoxyflavone	PubChem	44258544	C25H28O12
9	5-Hydroxy-7,8,2'-trimethoxyflavone	PubChem	44258542	C24H26O11
10	5-Hydroxy-7,8,2'-trimethoxyflavone 5-glucoside	PubChem	44258542	C24H26O11
11	Andrograpanin	PubChem	11666871	C20H30O3
12	Andrographidine A	PubChem	13963762	C23H26O10
13	Andrographidine C	PubChem	5318484	C23H24O10
14	Andrographidine E	PubChem	13963769	C24H26O11
15	Andrographin	PubChem	5318506	C18H16O6
16	Andrographolide	PubChem	5318517	C20H30O5
17	Andropanoside	PubChem	44575270	C26H40O9
18	Apigenin	PubChem	5280443	C15H10O5

ISSN 2515-8260 Volume 08, Issue 03, 2021

19	Apigenin 7,4'-dimethyl ether	PubChem	5281601	C17H14O5
20	Carvacrol	PubChem	10364	C10H14O
21	Carvacrol	PubChem	10364	C10H14O
22	CHEMBL479285	PubChem	11078630	C20H30O5
23	Citrostadienol	PubChem	9548595	C30H50O
24	Dehydroandrographoline	PubChem	71307452	C20H28O5
25	Deoxyandrographolide	PubChem	21679042	C20H30O4
26	Diterpene II (Lactone)	PubChem	339816	C20H26O5
27	Eugenol	PubChem	3314	C10H12O2
28	Hentriacontane	ChemSpider	12410	C31H64
29	MLS001143515	PubChem	10473975	C21H32O5
30	Myristic acid	PubChem	11005	C14H28O2
31	Neoandrographolide	PubChem	9848024	C26H40O8
32	Paniculide-A	PubChem	11821485	C15H20O4
33	Paniculide-B	PubChem	101289823	C15H20O5
34	Paniculide-C	PubChem	101289824	C15H18O5
35	Stigmasta-5,22-dien-3-ol	PubChem	53870683	C29H48O
36	Stigmasterol	PubChem	5280794	C29H48O
37	Tritriacontane	ChemSpider	12411	C33H68
38	Wogonin	PubChem	5281703	C16H12O5
39	Atovaquone	PubChem	74989	C22H19ClO3
40	Darunavir	PubChem	213039	C27H37N3O7S
41	dexamethasone	PubChem	5743	C22H29FO5
42	Favipiravir	PubChem	492405	C5H4FN3O2
43	Hydroxychloroquine	PubChem	3652	C18H26ClN3O
44	Ivermectin	DrugBank	DB00602	C95H146O28

ISSN 2515-8260 Volume 08, Issue 03, 2021

45	Nelfinavir	PubChem	64143	C32H45N3O4S
46	Ouabain	PubChem	439501	C29H44O12
47	Remdesivir	PubChem	121304016	C27H35N6O8P
48	Saquinavir	DrugBank	DB01232	C38H50N6O5

Table 2 : SARS-CoV2 target proteins and their corresponding grid parameters

S. No	Protein Name	Grid Box XYZ Coordinates Centre (Å)	Grid Spacing (Å)
1	Main Protease (NSP 5) (6LU7)	-23.435 2.670 51.241	0.375
2	Non-structural protein 9 (6WXD)	56.325 1.573 21.494	0.375
3	Envelope protein (5X29)	5.513 -0.464 6.602	0.375
4	ORF1a polyprotein (2G9T)	119.130 120.647 81.743	1.000
5	Receptor binding domain (6M0J)	-26.872 18.465 -9.269	1.000
6	Membrane protein (3I6G)	26.358 1.956 45.596	0.375
7	Non-structural protein 3 (6VXS)	-6.024 -20.209 -30.194	0.375
8	ORF3a Accessory protein (6XDC)	145.801 145.378 153.392	0.375
9	NSP15 (6VWW)	-70.519 22.297 -2.350	0.375
10	Spike Proteins (6CRV)	162.996 164.796 153.523	1.000

ISSN 2515-8260 Volume 08, Issue 03, 2021

Table 3: Lipinski rule of 5 for the selected phyto compounds

S. No	Compounds	Molecular Weight (g/mol)	LogP	#Rotatable Bonds	#Acceptors	#Donors
1	14-Deoxy-11,12-Didehydroandrographolide	332.44	2.72	3	4	2
2	14-Deoxy-11-Oxoandrographolide	348.439	1.89	4	5	2
3	14-Deoxyandrographolide	334.456	2.81	4	4	2
4	14-Deoxyandrographoside	496.597	0.48	7	9	5
5	2,4-Dihydroxycinnamic Acid	180.16	0.7	2	4	3
6	3-O-Caffeoyl-D-Quinic Acid	353.303	-1.05	4	9	5
7	5-Hydroxy-3,7,8-Trimethoxy-2-(2-Methoxyphenyl)-4H-Chromen-4-One	374.345	-0.12	5	8	2
8	5-Hydroxy-7,8,2',3'-Tetramethoxyflavone	358.346	0.4	5	7	1
9	5-Hydroxy-7,8,2'-Trimethoxyflavone	328.32	0.7	4	6	1

10	5-Hydroxy-7,8,2'-Trimethoxyflavone 5-Glucoside	490.461	-1.46	7	11	4
11	Andrograpanin	318.457	3.66	4	3	1
12	Andrographidine A	462.451	-0.99	6	10	4
13	Andrographidine C	460.435	-1.18	6	10	4
14	Andrographidine E	490.461	-1.46	7	11	4
15	Andrographin	328.32	0.7	4	6	1
16	Andrographolide	350.455	1.98	3	5	3
17	Andropanoside	496.597	0.48	7	9	5
18	Apigenin	270.24	0.52	1	5	3
19	Apigenin 7,4'-Dimethyl Ether	298.294	1.01	3	5	1
20	Carvacrol	150.22	2.76	1	1	1

21	Carvacrol	150.22	2.76	1	1	1
22	CHEMBL479285	350.455	1.98	3	5	3
23	Citrostadienol	426.729	6.82	5	1	1
24	Dehydroandrographoline	348.439	1.89	3	5	3
25	Deoxyandrographolide	334.456	2.81	4	4	2
26	Diterpene II (Lactone)	346.423	2.7	3	5	0
27	Eugenol	164.2	2.01	3	2	1
28	Hentriacontane	436.84	9.64	28	0	0
29	MLS001143515	364.482	2.2	5	5	2
30	Myristic Acid	228.37	3.69	12	2	1
31	Neoandrographolide	480.598	1.26	7	8	4

32	Paniculide-A	264.321	1.62	3	4	1
33	Paniculide-B	280.32	0.79	4	5	2
34	Paniculide-C	278.304	0.7	4	5	1
35	Stigmasta-5,22-Dien-3-Ol	412.702	6.62	5	1	1
36	Stigmasterol	412.702	6.62	5	1	1
37	Tritriacontane	464.89	10.01	30	0	0
38	Wogonin	284.267	0.77	2	5	2

Table 4: Docking scores of Compounds against COVID-19 proteins

(Bold ones indicate the ligands that do not satisfy the set threshold)

S. No	Compounds	Abbr	6LU7	6WXD	5X29	2G9T	6M0J	3I6G	6VXS	6XDC	6VWW	6CRV
1	14-Deoxy-11,12-Didehydroandrographolide	DDHA	**-6.8**	**-6.1**	-8.1	-7.2	-7.4	-9.1	**-6.7**	-7.2	-7	-8.6
2	14-Deoxy-11-Oxoandrographolide	DOA	**-6.9**	**-6.3**	-7.1	-7.5	-7.6	-7.9	-7.4	-7.4	**-6.9**	-8.8
3	14-Deoxyandrographolide	DLIDE	**-6.7**	**-6.4**	-7.3	-7.4	-7.6	-8.4	-7.1	-7.5	-7	-8.4
4	14-Deoxyandrographoside	DSID	-7.4	-7.4	-8.4	-7.8	-8.6	-9.4	-8.4	-7.9	-8.2	-9
5	2,4-Dihydroxycinnamic Acid	DHCA	**-6.1**	**-5.8**	**-5.8**	**-6.3**	**-6.6**	**-6.4**	**-6.1**	**-5.7**	**-6.1**	**-6.6**
6	3-O-Caffeoyl-D-Quinic Acid	CDQA	**-6.8**	**-6.9**	-7.3	-8.4	-7.9	-7.9	-7.3	-7.3	-7.4	-8.5
7	5-Hydroxy-3,7,8-Trimethoxy-2-(2-Methoxyphenyl)-4 H-Chromen-4-One	HTMCO	**-6.3**	**-6.2**	**-6.8**	-7.6	-7.4	-8.2	**-6.3**	**-6.9**	**-6.9**	-7.8
8	5-Hydroxy-7,8,2',3'-Tetramethoxyflavone	HTMF	**-6.2**	**-6.7**	-7.1	-7.3	-7.1	-7.8	**-6.8**	-7.1	-7.2	-8
9	5-Hydroxy-7,8,2'-Trimethoxyflavone	DT3MF	**-6.6**	**-6.6**	-7.1	-7.3	-8	-8.1	**-6.9**	-7.3	-7.4	-7.9
10	5-Hydroxy-7,8,2'-Trimethoxyflavone 5-Glucoside	HT5G	-7.3	-7.2	-8	-7.8	-8.6	-8.4	-7.9	-8.2	-8.8	-9.6
11	Andrograpanin	AGNIN	**-6.7**	**-6.4**	-7.5	-7.4	-7.4	-8.4	-7.1	-7.4	-7.1	-8.2
12	Andrographidine A	AGDA	-7.2	-7.6	-8.2	-8	-8.4	-9.1	-7.7	-8.6	-8.8	-9.3

13	Andrographidine C	AGDC	-7	-7.6	-8.4	-8	-8.3	-8.9	-7.8	-8.7	-8.8	-9.2
14	Andrographidine E	AGDE	-7	-7.2	-8.3	-8	-7.5	-8.9	-7.7	-8.4	-8.7	-8.5
15	Andrographin	AGPS	**-6.6**	**-6.6**	-7.4	-7.3	-8	-8.1	**-6.8**	-7.3	-7.4	-7.9
16	Andrographolide	APLD	**-6.5**	**-6.8**	-7.9	-7.4	-7.5	-8.6	-7.1	-7.5	-7.3	-8.4
17	Andropanoside	APSD	-7.3	-7.3	-8.3	-8.1	-8.4	-9.4	-7.7	-8	-8.2	-9
18	Apigenin	APGN	**-6.7**	-7.3	-7.6	-7.7	-7.8	-8.4	-7.8	-7.5	-8.1	-8.5
19	Apigenin 7,4'-Dimethyl Ether	APNDE	**-6.8**	-7.4	-7.9	-7.5	-7.8	-8.3	-7.9	-7.4	-7.9	-8.1
20	Carvacrol	CARV	**-5.3**	**-5.8**	**-6**	**-5.6**	**-6.1**	**-6.1**	**-5.7**	**-5.4**	**-5.4**	**-6.5**
21	Carvacrol	CARV1	**-5.3**	**-5.8**	**-6**	**-5.6**	**-6.1**	**-6.1**	**-5.7**	**-5.4**	**-5.4**	**-6.5**
22	Chembl479285	CHEL	**-6.3**	**-6.7**	-7.5	-7.4	-7.6	-9	-7.1	-7.5	-7.4	-8.4
23	Citrostadienol	CITRO	-7.2	-8	-9	-8.2	-8.7	-9.8	-7.8	-8.2	-7.8	-9
24	Dehydroandrographoline	DEHA	**-6.4**	**-6.4**	-7.5	-7.5	-7.5	-8.6	**-6.7**	-7.6	-7.2	-8.4
25	Deoxyandrographolide	DLIDE	**-6.9**	**-6.7**	-7.2	-7.3	-7.1	-9.1	**-6.9**	-7.8	-7	-8.4
26	Diterpene II (Lactone)	DPENE	-7.4	**-6.9**	-8.2	-8.4	-8.6	-9	-7.8	-7.4	-8	-8.8
27	Eugenol	EUGN	**-5.5**	**-5.4**	**-5.9**	**-5.9**	**-5.9**	**-5.8**	**-5.2**	**-5.1**	**-5.2**	**-6.1**
28	Hentriacontane	HENT	**-3.7**	**-4.2**	**-6**	**-4.5**	**-4.8**	**-5.6**	**-4.6**	**-4.4**	**-4.5**	**-5.6**

29	Mls001143515	MLS	**-6.3**	**-5.7**	-7.4	-7	**-6.6**	-7.6	-7.1	-7.2	-7.3	-8.6
30	Myristic Acid	MYCD	**-4.7**	**-5.1**	**-5.3**	**-4.6**	**-5.1**	**-5.1**	**-4.3**	**-4.9**	**-4.4**	**-5.5**
31	Neoandrographolide	NAPLD	-7.5	-7.2	-8.4	-7.9	-8.8	-9.2	-7.6	-8.3	-8.1	-9.1
32	Paniculide-A	PAN A	**-6.2**	**-6**	**-6.7**	**-6.8**	-7.2	-7.7	**-6.3**	**-6.5**	**-6.5**	-7.7
33	Paniculide-B	PAN B	**-6.1**	**-6.8**	**-6.8**	**-6.4**	**-6.9**	-7.5	**-6.3**	**-6.8**	**-6.5**	-7.2
34	Paniculide-C	PAN C	**-6.2**	**-6.4**	-7.1	**-6.7**	-7.2	-7.5	**-6.5**	**-6.8**	**-6.2**	-7.6
35	Stigmasta-5,22-Dien-3-Ol	ST5OL	-7.8	-8.4	-9.1	-7.9	-8.7	-9.9	-7.6	-7.9	-7.8	-8.8
36	Stigmasterol	STIGOL	-7.8	-8.4	-9.1	-7.8	-8.8	-9.9	-7.7	-7.9	-7.8	-9.6
37	Tritriacontane	TRIT	**-3.9**	**-4.2**	**-5.9**	**-4.5**	**-4.7**	**-5.9**	**-4.6**	**-4.5**	**-4**	**-5.2**
38	Wogonin	WOGN	**-6.8**	**-6.7**	-7.6	-7.2	-8.2	-8.1	-7.6	-7.9	-7.9	-8.3

ISSN 2515-8260 Volume 08, Issue 03, 2021

Table 5: Docking scores of the repurposed drugs.

S.No	Positive Controls	Abbreviated Form	6LU7	6WXD	5X29	2G9T	6M0J	3I6G	6VXS	6XDC	6VWW	6CRV
1	Atovaquone	AVQ	-7.9	-8.9	-9.5	-8.5	-8.6	-9.7	-8.8	-8.6	-5.4	-8.8
2	Darunavir	DRV	-6.7	-7.6	-8.4	-7.7	-8.2	-8.2	-7.9	-7.6	-7.7	-9.1
3	dexamethasone	DEXM	-7.8	-6.9	-7.8	-8.2	-8.5	-9.2	-7.4	-7.3	-7.6	-8.6
4	Favipiravir	FAVP	-5.7	-5	-4.7	-6.1	-6.5	-5.4	-5.2	-5.4	-8.6	-6.3
5	Hydroxychloroquine	HCQ	-5.6	-6	-6.4	-6.1	-6.4	-7.1	-5.9	-6.1	-6.1	-7.1
6	ivermectin	IVMEC	-9.1	-7.9	-11.4	-9.1	-9.5	-10.7	-8.8	-8.4	-11.1	-11.6
7	Nelfinavir	NLFV	-8.1	-7.8	-9.9	-8.6	-9.2	-9.2	-8.4	8.5	-8.8	-9.8
8	Ouabain	OUA	-7.5	-6.8	-8	-8.7	-8.1	-8.7	-7.3	-8.9	-9	-8.7
9	remdesivir	REMD	-7	-7.1	-7.9	-7.9	-8.5	-8.7	-7.7	-8.1	-8.5	-9
10	Saquinavir	SAQV	-8.8	-7.9	-9.9	-7.8	-9.9	-10.5	-9.7	-9.9	-8.5	-9.7

Table 6: Binding interactions of the top scoring protein-ligand complexes

(Bold ones indicate the common amino-acid residues between the phytocompounds and the repurposed drugs against the viral proteins)

S.No	Protein-ligand complex	Hydrophobic interactions	Hydrogen bond interactions with distance(Å)
01	6LU7 - Stigmasterol complex	**Arg131**, **Thr199**, Tyr237, **Tyr239**, Leu271, Leu272, Gly275, Met276, **Leu286**, Leu287	Asp289 -> 3.15
02	6LU7 - Stigmasta-5,22-dien-3-ol complex	**Arg131**, **Thr199**, Tyr237, **Tyr239**, Leu271, Leu272, Gly275, Met276, **Leu286**, Leu287	Asp289 -> 3.17
03	6LU7 - Ivermectin complex	**Arg131**, Lys137, Thr169, Ala193, Ala194, Thr196, Asp197, Thr198, **Thr199**, Asn238, **Tyr239**, **Leu286**, Glu288	Leu287 -> 2.86
04	6WXD - Stigmasterol complex	**Arg39**, **Phe40**, Val41, **Phe56**, **Pro57**, Lys58, Ser59, **Ile65**, **Thr67**, **Ile91**, Leu94	Gly93 -> 3.14
05	6WXD - Stigmasta-5,22-dien-3-ol complex	**Arg39**, **Phe40**, Val41, **Phe56**, **Pro57**, Lys58, Ser59, **Ile65**, **Thr67, Ile91**, Leu94	Gly93 -> 3.17
06	6WXD - Atovaquone complex	**Arg39**, **Phe40**, **Phe56**, **Pro57**, **Ile65**, **Thr67, Ile91**, Lys92	Val41 -> 3.22 and 3.06
07	5X29 - Stigmasterol complex	Leu27, Leu28, **Leu31**, Ala32, Thr35, Ala40, Ile46, **Leu51**, **Pro54, Tyr57**	Arg61 -> 3.06, 3.30
08	5X29 - Stigmasta-5,22-dien-3-ol complex	**Leu31**, Thr35, Ala40, Ala43, Ala44, Val47, **Leu51**, **Pro54, Tyr57**, Ser60	Ser50 -> 3.28 and Ile46 -> 2.90
09	5X29 - Ivermectin complex	Phe20, Phe23, Val25, Leu27, Leu28, Val29, Thr30, **Leu31**, Ala32, Ile46, Val47, **Leu51**, **Pro54, Tyr57**, Arg61, Asn64, Leu65	Nil
10	2G9T - Diterpene II (Lactone)	Asn10, Phe16, Ala20, Val21, Asp22, Ala26,	Ala -> 2.98, Ser11 -> 2.88, Lys25 -> 3.09

		Asn40, Glu60	and Thr58 -> 2.95
11	2G9T - 3-O-caffeoyl-D-quinic acid complex	Val42, Gly69, Lys93, Tyr96	Val21 -> 3.06, 2.92, Val57 -> 2.92, Gly70 -> 2.89, Ala71 -> 3.35, Ser72 -> 2.81, Gly94 -> 2.84 and Lys95 -> 2.81,
12	2G9T - Ivermectin complex	Phe16, Ala20, Val21, Lys25, Asp29, Thr39, Asn40, Val42, Thr47, Thr49, Thr58, Pro59, Met63, Thr101	Nil
13	6M0J - Neoandrographolide complex	Phe40, Ser44, Ser47, Asn51, Thr347, Ala348, Trp349, Asp350, Arg393, His401	Asp382 -> 2.76 and Tyr385 -> 2.90
14	6M0J - Stigmasterol complex	Phe40, Leu73, Ala99, Leu100, Asn103, Asp350, Tyr385, Phe390, Leu391, Arg393	Ser77 -> 3.17 and Gln102 -> 2.84
15	6M0J - Saquinavir complex	Phe40, Ser44, Trp69, Leu73, Thr347, Trp349, Gly352, His378, Tyr385, Leu391, Arg393, Phe390, His401	Asp382 -> 3.06, Ala384 -> 2.82 and Asn394 -> 2.94
16	3I6G - Stigmasta-5,22-dien-3-ol complex	Phe8, Tyr26, Tyr27, Asp29, Asp30, Ser52, Tyr63, Leu65, Met98, Ala211, Pro235, Phe241	Arg6 -> 3.06
17	3I6G - Stigmasterol complex	Phe8, Tyr26, Tyr27, Asp29, Asp30, Ser52, Tyr63, Leu65, Met98, Ala211, Pro235, Phe241	Arg6-> 3.08
18	3I6G - Ivermectin complex	Arg6, Phe8, Tyr26, Asp29, Asp30, Phe56, Ser57, Lys58, Tyr63, Glu212, Leu230, Val231, Glu232	Ser4 -> 2.70, Thr233 -> 3.12 and Lys243 -> 2.82
19	6VXS- 14-Deoxyandrographoside complex	Asp22, Ala38, Gly47, Gly48, Pro125, Ala129, Val155, Phe156, Gly130, Ile131, Phe132	Val49 -> 2.95, Ile23 -> 2.99, Ala50 -> 3.15, Leu126 -> 2.85, Ala154 -> 2.73,2.90
20	6VXS - Saquinavir complex	Asp22, Ile23, Ala38, Asn40, Lys44, Gly46, Gly47, Gly48, Val49, Leu127, Ala129, Ile131, Phe132, Val155, Asp157, Leu160	Leu126 -> 2.98, Ser128 -> 2.93, Phe156 -> 3.28

21	6XDC - Andrographidine C complex	Lys61, Ile62, Thr64, Lys66, Ser205 Phe207, Thr208	Ile63 -> 3.12 and 2.74, Arg122 -> 2.95, Arg126 -> 3.26, Asp142 -> 3.01, Tyr206 -> 2.70
22	6XDC - Saquinavir complex	Thr64, Leu65, Leu71, Lys75, His78, Arg122, Arg126, Tyr141, Asp142, Ala143, Asn144, Asn161, Tyr189, Tyr206	Asp142 -> 3.10, 3.04, 3.07, Tyr189 -> 2.84
23	6VWW - Andrographidine C complex	Asn29, Asn30, Pro51	Asn30 -> 2.77, 3.14, Asn46-> 2.99, Thr48 -> 2.76, Leu50 ->3.16, 2.70
24	6VWW - Ivermectin complex	Ile27, Ile28, Asn30, Asn46, Thr48, Thr49, Leu50, Pro51	Asn29 -> 3.03, Asn30 -> 3.08
25	6CRV - Stigmasterol complex	Tyr738, Phe741, Phe952, Arg977, Thr980, Gly981, Leu983, Gln984, Ser985	Asp976 -> 3.24
26	6CRV - Ivermectin complex	Ile299, Gln301, Pro651, Arg747, Ala748, Ser750, Gly751, Ala753, Ala754, Asp757, Leu843, Gln939, Leu994	Lys715 -> 3.28, Gln936 -> 2.83

Table 7: ADMET Predictions for the screened phytocompounds

S. No	Phytocompounds	Water solubility (log	Intestinal Absorption (%	Blood Brain Barrier Permeabil	CYP3A4 substrate (Yes/No)	CYP3A4 inhibitior (Yes/No)	Total Clearance (log	MRTD (log mg/kg/	Acute Oral Rat Toxicity LD50
1	14-Deoxy-11,12-Didehydroandrographolide	-3.878	97.152	0.024	Yes	No	1.217	-0.022	2.017
2	14-Deoxyandrographolide	-3.954	96.646	-0.003	Yes	No	1.175	-0.019	2.053
3	14-Deoxyandrographoside	-3.562	50.309	-1.168	No	No	1	-0.123	2.51
4	5-Hydroxy-3,7,8-Trimethoxy-2-(2-Methoxyphenyl)-4H-Chromen-4-One	-3.411	96.276	-0.873	Yes	Yes	0.658	0.058	2.193
5	5-Hydroxy-7,8,2',3'-Tetramethoxyflavone	-3.735	95.701	-0.787	Yes	Yes	0.388	0.189	2.36
6	5-Hydroxy-7,8,2'-Trimethoxyflavone	-3.547	95.965	-0.615	Yes	No	0.374	0.143	2.113
7	5-Hydroxy-7,8,2'-Trimethoxyflavone 5-Glucoside	-3.485	66.379	-1.641	No	No	0.317	0.617	2.745
8	Andrograpanin	-4.923	96.632	-0.002	Yes	No	1.115	-0.973	2.157
9	Andrographidine A	-3.884	73.042	-1.408	No	No	0.439	**0.495**	2.83
10	Andrographidine C	-3.388	61.885	-1.433	No	No	0.41	0.555	2.918
11	Andrographidine E	-3.485	66.379	-1.641	No	No	0.317	0.617	2.745

12	Andrographin	-3.547	95.965	-0.615	Yes	No	0.374	0.143	2.113
13	Andrographolide	-3.494	95.357	-0.598	Yes	No	1.183	0.128	2.162
14	Andropanoside	-3.562	50.309	-1.168	No	No	1	-0.123	2.51
15	Apigenin	-3.329	93.25	-2.061	No	No	0.566	0.328	2.45
16	Apigenin 7,4'-Dimethyl Ether	-3.714	95.453	-0.458	Yes	Yes	0.737	0.193	2.085
17	CHEMBL479285	-3.494	95.357	-0.598	Yes	No	1.183	0.128	2.162
18	Citrostadienol	-6.662	94.878	0.782	Yes	No	0.585	-0.578	2.56
19	Dehydroandrographoline	-3.85	92.953	-0.741	Yes	No	1.075	0.097	2.34
20	Deoxyandrographolide	-3.885	95.5	0.06	Yes	No	1.163	0.007	2.52
21	Diterpene II (Lactone)	-3.797	100	-0.326	Yes	No	0.968	0.096	2.006
22	MLS001143515	-3.858	96.262	-0.393	Yes	No	1.067	0.217	2.153
23	Stigmasta-5,22-Dien-3-Ol	-6.682	94.97	0.771	Yes	No	0.618	-0.664	2.54
24	Stigmasterol	-6.682	94.97	0.771	Yes	No	0.618	-0.664	2.54
25	Wogonin	-3.469	92.682	-0.232	Yes	Yes	0.294	0.151	2.265

ISSN 2515-8260 Volume 08, Issue 03, 2021

Table 8: Relative binding affinity of Ligand 34 with SARS-CoV2 target proteins

S. No	Protein Name	dG bind (kcal/mol)
01	Main Protease (NSP 5) (6LU7)	-42.27616016
02	Non-structural protein 9 (6WXD)	-67.2520591
03	Envelope protein (5X29)	-69.61830806
04	ORF1a polyprotein (2G9T)	-57.73277917
05	Receptor binding domain (6M0J)	-31.53933377
06	Membrane protein (3I6G)	-61.11321444
07	Non-structural protein 3 (6VXS)	-90.71231119
08	ORF3a Accessory protein (6XDC)	-48.86515207
09	NSP15 (6VWW)	-42.76920382
10	Spike Proteins (6CRV)	-48.82635419

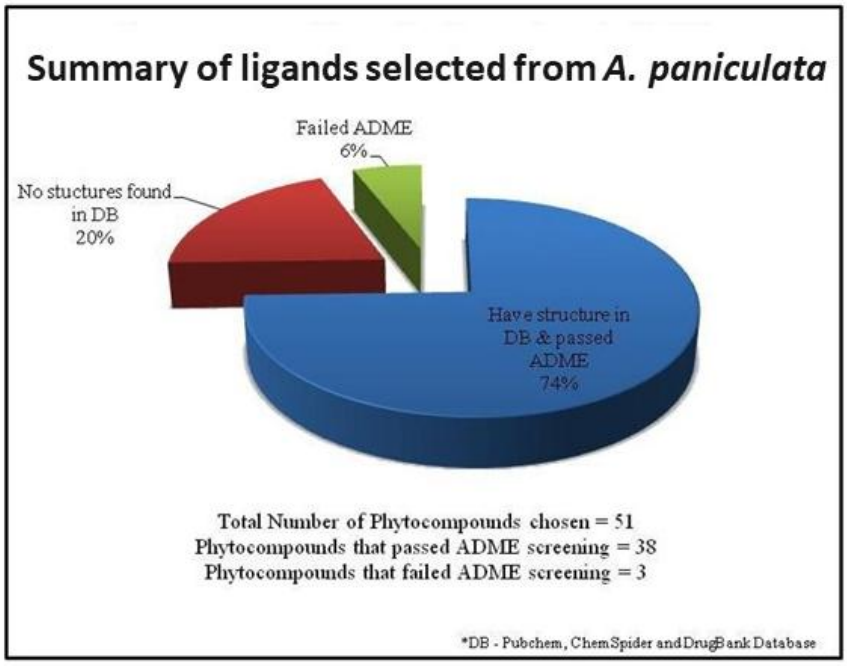

Figure 1: Summary of ligands selected from *A. paniculata*

ISSN 2515-8260 Volume 08, Issue 03, 2021

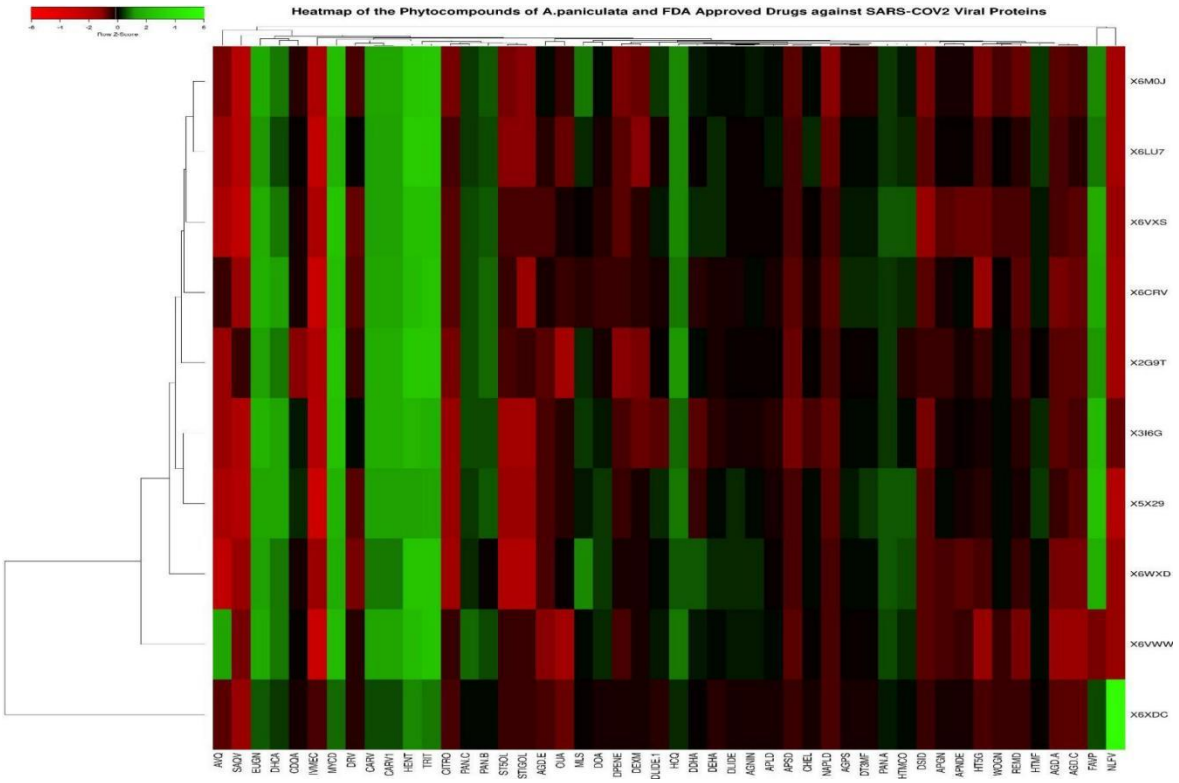

Figure 2: Heatmap of the Phytocompounds of A.paniculata and FDA Approved Drugs against SARS-COV2 Viral Proteins (Mentioned in PDB ID)

Abbreviations:

A.paniculata **phytocompounds:1) DDHA**: 14-Deoxy-11,12-Didehydroandrographolide, **2) DOA**: 14-Deoxy-11-Oxoandrographolide, **3) DLIDE**: 14-Deoxyandrographolide, **4) DSID**: 14-Deoxyandrographoside, **5) DHCA**: 2,4-Dihydroxycinnamic Acid, **6) CDQA**: 3-O-Caffeoyl-D-Quinic Acid, **7) HTMCO**: 5-Hydroxy-3,7,8-Trimethoxy-2-(2-Methoxyphenyl)-4H-Chromen-4-One, **8) HTMF**: 5-Hydroxy-7,8,2',3'-Tetramethoxyflavone, **9) DT3MF**: 5-Hydroxy-7,8,2'-Trimethoxyflavone, **10) HT5G**: 5-Hydroxy-7,8,2'-Trimethoxyflavone 5-Glucoside, **11) AGNIN**: Andrograpanin, **12) AGD A**: Andrographidine A, **13) AGD C**: Andrographidine C, **14) AGD E**: Andrographidine E, **15) AGPS**: Andrographin, **16) APLD**: Andrographolide, **17) APSD**: Andropanoside, **18) APGN**: Apigenin, **19) APNDE**: Apigenin 7,4'-Dimethyl Ether, **20) CARV**: Carvacrol, **21) CARV1**: Carvacrol, **22) CHEL**: Chembl479285, **23) CITRO**: Citrostadienol, **24) DEHA**: Dehydroandrographoline, **25) DLIDE**: Deoxyandrographolide, **26) DPENE**: Diterpene II (Lactone), **27) EUGN**: Eugenol, **28) HENT**: Hentriacontane, **29) MLS**: MLS001143515, **30) MYCD**: Myristic Acid, **31) NAPLD**: Neoandrographolide, **32) PAN A**: Paniculide-A, **33) PAN B**: Paniculide-B, **34) PAN C**: Paniculide-C, **35) ST5OL**: Stigmasta-5,22-Dien-3-Ol, **36) STIGOL**: Stigmasterol, **37) TRIT**: Tritriacontane, **38) WOGN**: Wogonin, **39) AVQ:** Atovaquone, **40) DRV:** Darunavir, **41) DEXM:** Dexamethasone, **42) FAVP:** Favipiravir, **43) HCQ:** Hydroxychloroquine, **44) IVMEC:** Ivermectin, **45) NLFV:** Nelfinavir, **46) OUA:** Ouabain, **47) REMD:** Remdesivir, **48) SAQV:** Saquinavir

ISSN 2515-8260 Volume 08, Issue 03, 2021

Viral Proteins: 1) 6LU7: Main Protease (NSP 5), **2) 6CRV:** Spike Proteins, **3) 5X29**: Envelope protein, **4) 3I6G:** Membrane protein, **5) 6M0J:** Receptor binding domain, **6) 6XDC:** ORF3a Accessory protein, **7) 6VWW:** NSP15, **8) 2G9T:** ORF1a polyprotein, **9) 6VXS:** Non-structural protein 3, **10) 6WXD:** Non-structural protein 9

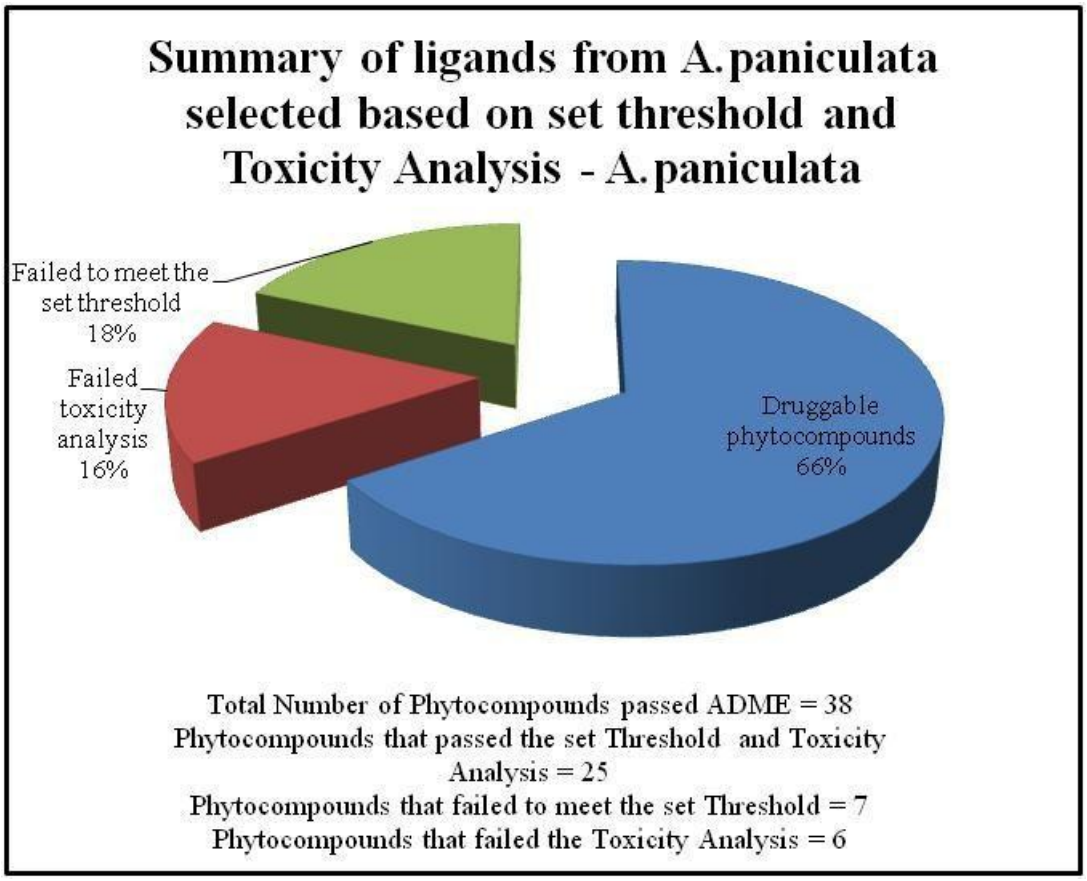

Figure 3: Representation of ligands selected based on the set threshold and toxicity profile of *A.paniculata*

ISSN 2515-8260 Volume 08, Issue 03, 2021

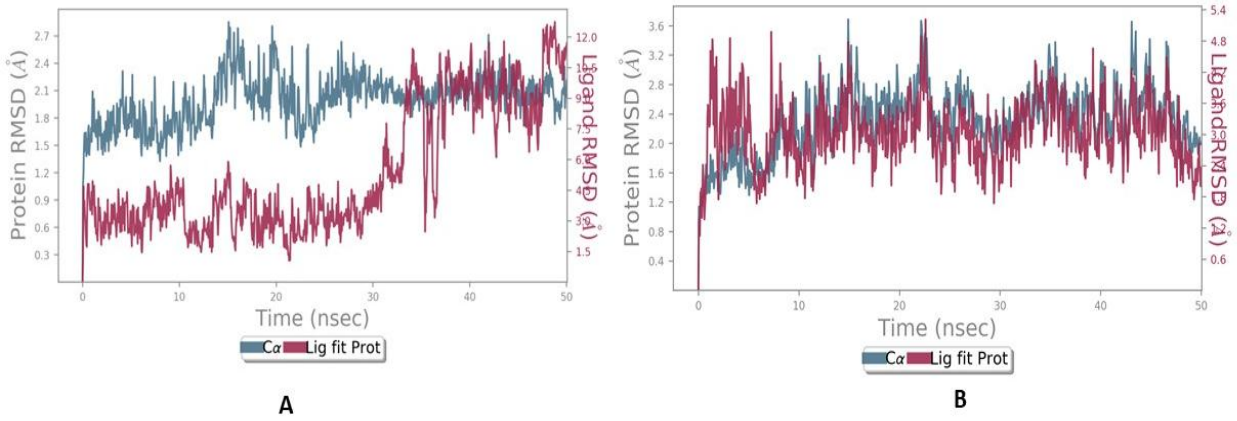

Figure 4 RMSD Profile of Protein: Ligand complexes A.Main protease (PDB ID: 6LU7): Stigmasterol B.Receptor binding domain (PDB ID: 6M0J) : Stigmasterol

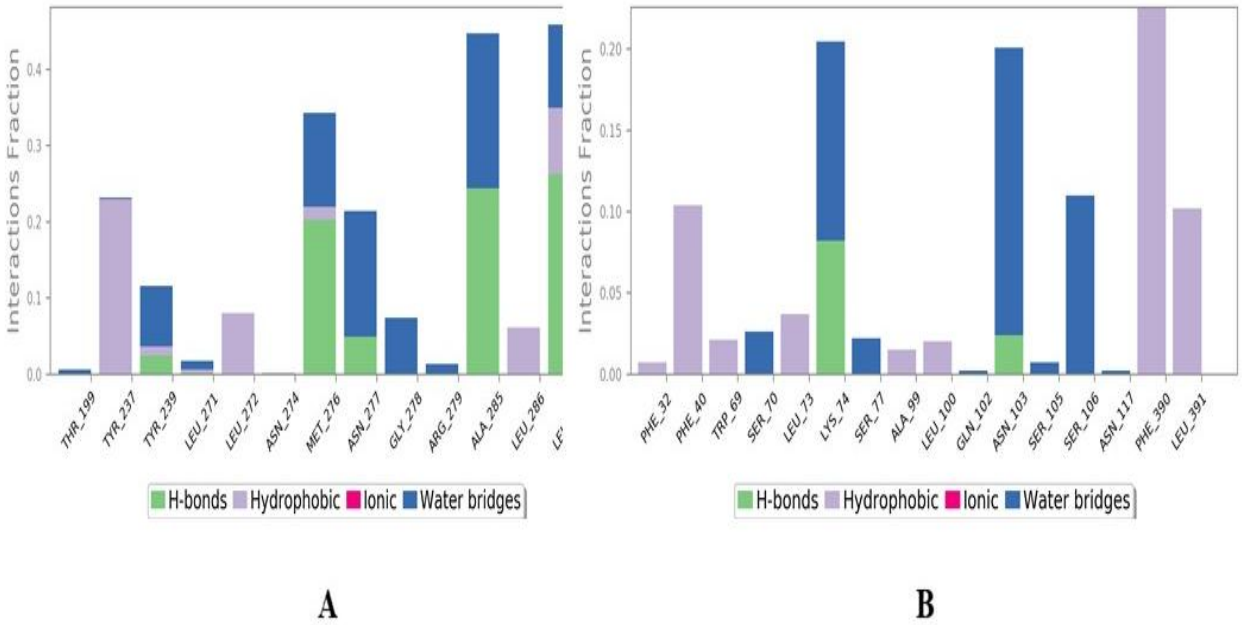

Figure 5 Protein: ligand Contacts A. Main protease (PDB ID: 6LU7) : Stigmasterol B. Receptor binding domain (PDB ID: 6M0J): Stigmasterol

ISSN 2515-8260 Volume 08, Issue 03, 2021

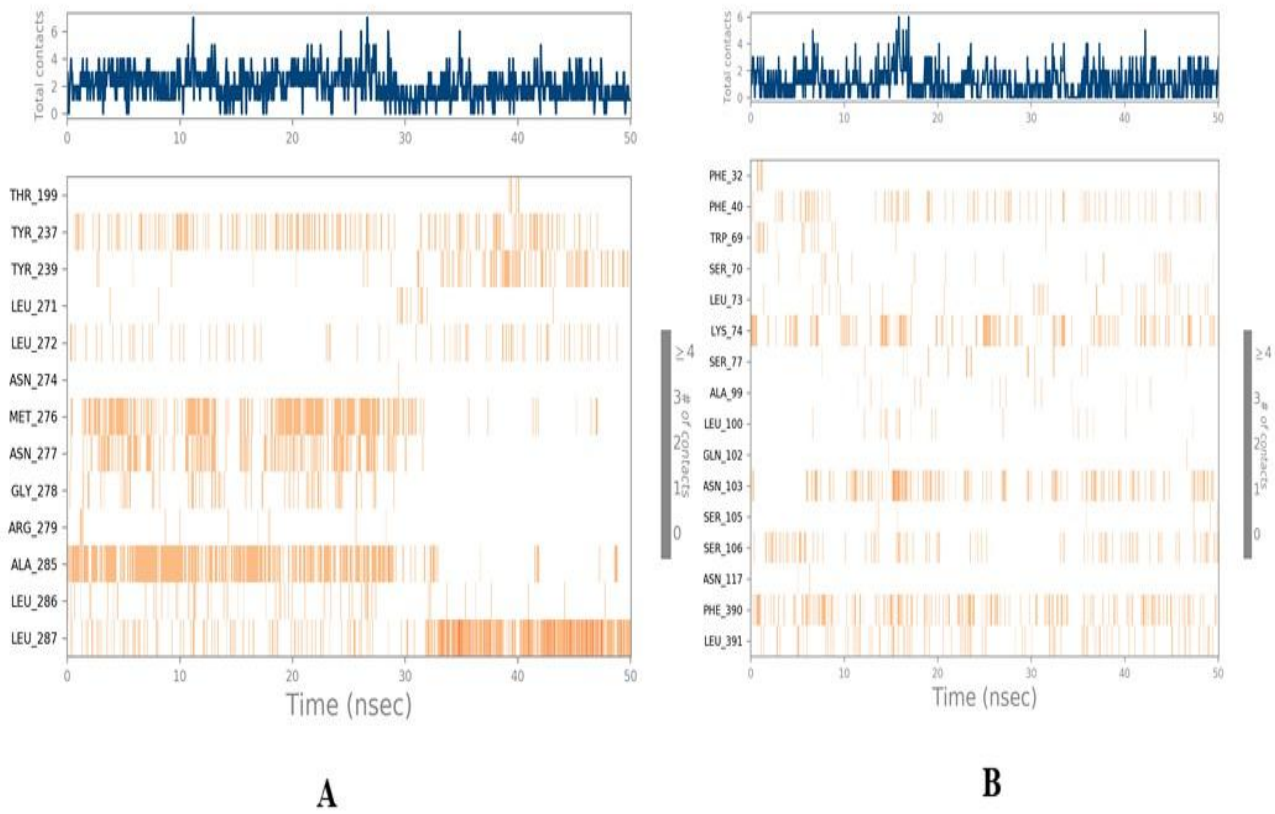

Figure 6 Timeline representation of Protein: Ligand Complex A. Main protease: Stigmasterol B. Receptor binding domain: Stigmasterol